Supplementary Information (SI) for Soft Matter.
This journal is © The Royal Society of Chemistry 2025

Supplementary Information for Crystallization of non-convex colloids: the roles of particle shape and entropy

Johnathon P. Gales,[†] Min Jae Kim,[‡] Glen M. Hocky,[¶] and David J. Pine[*,†,‡]

†*Department of Physics, New York University, New York, NY 10003, USA*

‡*Department of Chemical and Biomolecular Engineering, New York University, New York, NY 11201, USA*

¶*Department of Chemistry and Simons Center for Computational Physical Chemistry, New York University, New York, NY 10003, USA*

E-mail: pine@nyu.edu

1 Simulation Methods

Simulations are performed using HOOMD-Blue.[1] First, we define the fundamental simulation units of energy, distance, and mass. We choose energy to be in units of $k_{\mathrm{B}}T$, distance to be in units of diamond lattice constant a, and mass to be in units of our particle masses m_p. All other units are derived from these three fundamental units. Tetrahedral lobed patchy particles (TLPPs) are defined within HOOMD-Blue by nine spheres: The first sphere is at the cluster's center of mass and applies a rigid body constraint to the four spheres that act as the cluster's lobes and patches. The size of the spheres varies to achieve the desired compression ratio and size ratio for the cluster. Each cluster has equal mass 1 m_p and experiences gravity as a constant force in the vertical z-direction with a magnitude of $F_g = -0.025k_{\mathrm{B}}T/a$. 2400

tetrahedra are initially evenly spaced in a $4 \times 4 \times 375$ size simulation box.

Cluster positions are evolved using Langevin dynamics with a temperature $T = 1$, a time step of Δt=0.00005, and a friction coefficient of γ=1. The patch particles interact with each other through an attractive Wang-Frenkel potential with $\epsilon = 10 k_{\mathrm{B}} T$ to mimic the real particles' DNA brush interactions. The lobe particles interact with each other through a weak attractive Wang-Frenkel potential with $\epsilon = 1$ to mimic the depletion interaction caused by surfactant micelles present in experiment.

The hard walls at the top and bottom of the simulation box interact with all particles via a purely repulsive Lennard-Jones potential:

$$V_{wall}(r) = 4\epsilon \left[\left(\frac{\sigma}{r} \right)^{12} - \alpha \left(\frac{\sigma}{r} \right)^{6} \right] \tag{1}$$

where

$$\alpha = 0 \, . \tag{2}$$

The template particles on the bottom surface are identical to the particles in solution, except they can not move. The presence of the template seeds the crystal, making the nucleation less stochastic for nearly all geometries. For this reason, we run only a single long simulation at each geometry for compression ratios 0.725 and below. At compression 0.75, six parallel simulations were employed to verify the lack of crystallization for all but the largest size ratios.

2 Spherical Patchy Particles

For comparison to the TLPPs, we simulate the assembly of spherical patchy particles. The spherical particles' patch-patch interactions are equivalent to the tetrahedral particles' patch-patch interactions. The body-body interactions are equivalent to the tetrahedral tetrahedra's lobe-lobe interactions. After assembly, the correlation function $g(r)$ is calculated and plotted

in 1. The structure has a significant peak at the position of diamond's 1st nearest neighbors (which is just the particle diameter), a small peak at the second nearest neighbor position, and no further correlations, indicating an amorphous structure. Additionally, there is no liquid peak, as most spherical patchy particles are bound.

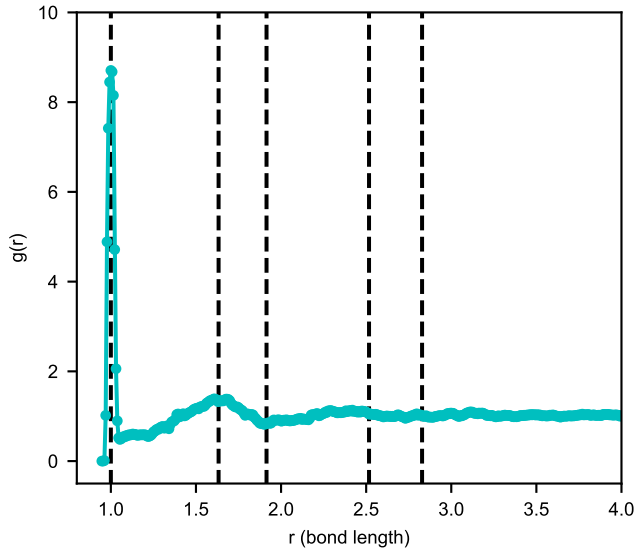

Figure 1: The pair distribution function $g(r)$ for an assembly of spherical patchy particles.

3 Torsion Standard Deviations

For comparison to the phase diagram in the main text, we plot the torsion angle distribution standard deviations for compression ratios 0.60, 0.65, 0.70, and 0.725 in SI Fig. 2. It can be seen that the torsion angles transition from low standard deviations to large standard deviations at the same geometries where the pair correlations transition from crystal to amorphous. Additionally, this plot shows that the interlock itself becomes looser for less compressed clusters, as their degree of concavity decreases.

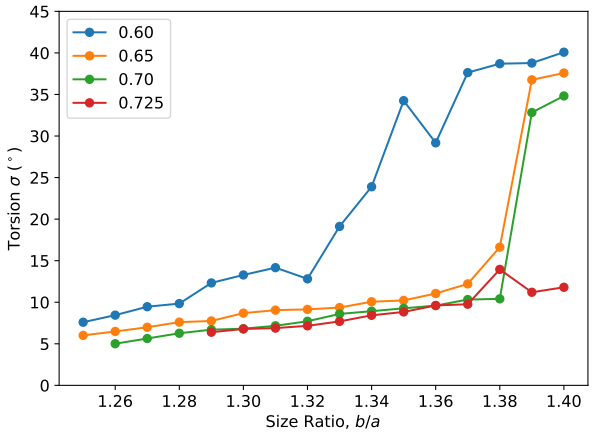

Figure 2: Torsion standard deviations for compression ratios 0.60, 0.65, 0.70, and 0.725

4 Representative Histogram of Distances

Two spring constants are used for the umbrella sampling simulations. A stronger spring constant of 3265 $k_BT/\mu\text{m}^2$ is used for sampling near the patch-patch interaction-well distance (from $\xi_0 = 1.25\mu\text{m}$ to $\xi_0 = 1.37$ μm. A weaker spring constant of 326.5 $k_BT/\mu\text{m}^2$ is used for sampling far away from the patch-patch distance. The width of the histogram distribution at a fixed ξ_0 represents the strength of the spring. Far from the bonding distance, the distribution is wide due to the weaker spring constant, while the distribution is tighter near the bonding distance due to the stronger spring constant.

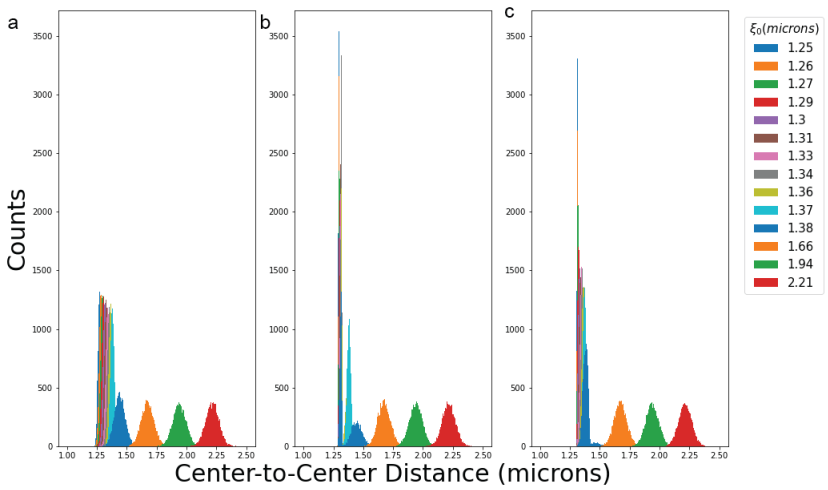

Figure 3: Histogram of the center-to-center distance between two tetrahedra interacting via patch-patch WF potential. a. SR = 1.15. b. SR = 1.30. c. SR = 1.40. At an SR (1.15) in which the geometry of the cluster precludes the patch-patch contact, the statistics of distances at interlock distance are uniform. At an SR for which the patch-patch contact is possible, the tetrahedra prefer distances within the the patch-patch interaction minima, which is indicated by higher statistics at the patch-patch contact distance. At a higher SR, the tetrahedra explore distances closer than the expected patch-patch interaction-minima distance. This is due to the bending of the bonds.

5 Spherical Particle Interacting via WF Potential

Histograms from umbrella sampling for two TLPPs interacting via a WF potential are shown in Figure 4. The sampling of the center-to-center distance properly captures the well depth of $10k_{\mathrm{B}}T$ and width of 20 nm.

The free energy matches the input WF potential as shown in Figure 4b. However, the free energy increases slightly as the two particles are brought closer together. This is due to the decrease in the entropy when two particles are confined to a smaller distance.

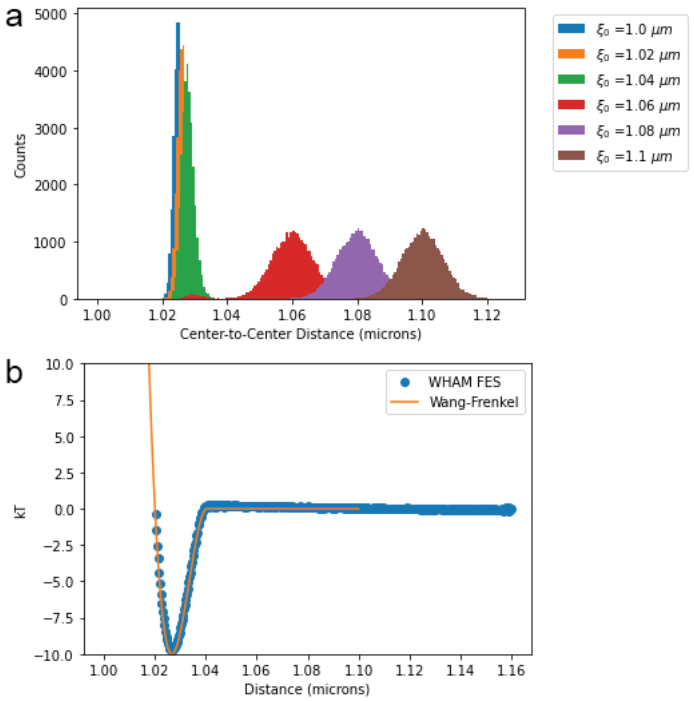

Figure 4: a. Histogram of the center-to-center distance between two spheres interacting via WF potential. b. Resulting free energy surface from the US sampling using WHAM algorithm.

6 Entropy of 2 Tetrahedra

Since the umbrella sampling measures the free energy of only two tetrahedra interactions, it has contributions only from the particles' interactions and their entropy. Since our particles interact with a Wang-Frenkel interaction that cuts off at $r > r_c$, we know that at distances beyond the attractive well, the free energy is simply the entropic cost of bringing two tetrahedra together. To verify this and find the entropy at short distances, we can find the free energy of two particles whose attractive WF interactions have been replaced with a purely repulsive potential, modeling a non-binding polymer brush as in Hueckel et al. [2] as shown in Equation 3. The parameters r, L, and σ are the particle radius, polymer brush height (10 nm), and polymer brush density (0.09 nm^{-2}), respectively. Figure 5 shows the free energy of the purely entropic system for three different particle geometries. The entropic cost of bringing two clusters closer increases slowly at long distances and then very quickly at short

distances, where they are required to interlock, and their translational and rotational degrees of freedom are restricted.

$$\frac{V_{brush}(r)}{k_B T} = \frac{16\pi r L^2 \sigma^{3/2}}{35}\left\{28\left[\left(\frac{2L}{h}\right)^{1/4} - 1\right] + \frac{20}{11}\left[1 - \left(\frac{h}{2L}\right)^{11/4}\right] + 12\left(\frac{h}{2L} - 1\right)\right\} \quad (3)$$

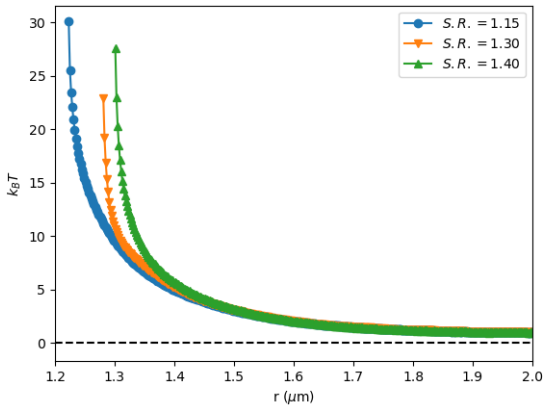

Figure 5: Free energy of two TLPPs with only repulsive brush interactions at three different TLPP geometries with compression ratio $d_{cc}/2a = 0.7$ and size ratios $b/a = 1.15$ (blue), $b/a = 1.30$ (orange), and $b/a = 1.40$ (green). Since there is no attractive patch-patch interaction this free energy is due entirely to the entropy of bringing two tetrahedra together

7 All Free Energies

The compression ratio (CR) and the size ratio (SR) affect the free energy of binding between a pair of tetrahedra. Umbrella sampling simulations were done for various combinations of CRs and SRs. The free energy barrier to binding and the local free energy minima are extracted from the free energy curve as shown in Figure 6 and Figure 7.

From Figure 6, the free energy barrier to bind decreases monotonically as a function of size ratio across all of the CRs. The free energy barrier significantly shifts down as the CR decreases. With decreasing CRs, the interlock mechanism becomes weaker; the facets of the tetrahedra become flatter. Furthermore, as the lobes are compressed into each other,

the lobe-lobe contact distance at larger separation distance becomes smaller. Therefore, the orientation of the tetrahedra are restricted (decrease in entropy) at a smaller separation distance than the cluster with larger CR.

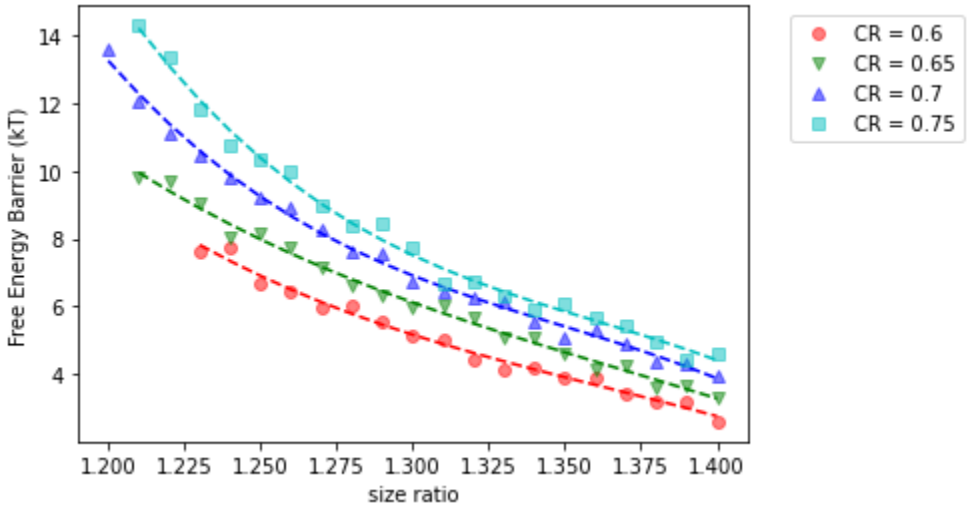

Figure 6: Free energy barrier of binding for various compression ratios (CRs). Across all of the CRs, the free energy barrier monotonically decreases as the size ratio increases. The free energy barrier shifts down as the tetrahedra become more compressed (decreasing compression ratio).

The local free energy minima values decrease with increasing SRs due to the lower entropy barrier of binding as shown in Figure 7. As the SR is increased, the difference in the local free energy minima between various CRs is diminished. When the bonds are formed at a larger size ratio, they can bend, and the tetrahedra prefer to explore the distances allowed by the bending of the bond. As a result, the free energy well does not get deeper but gets wider, as previously mentioned.

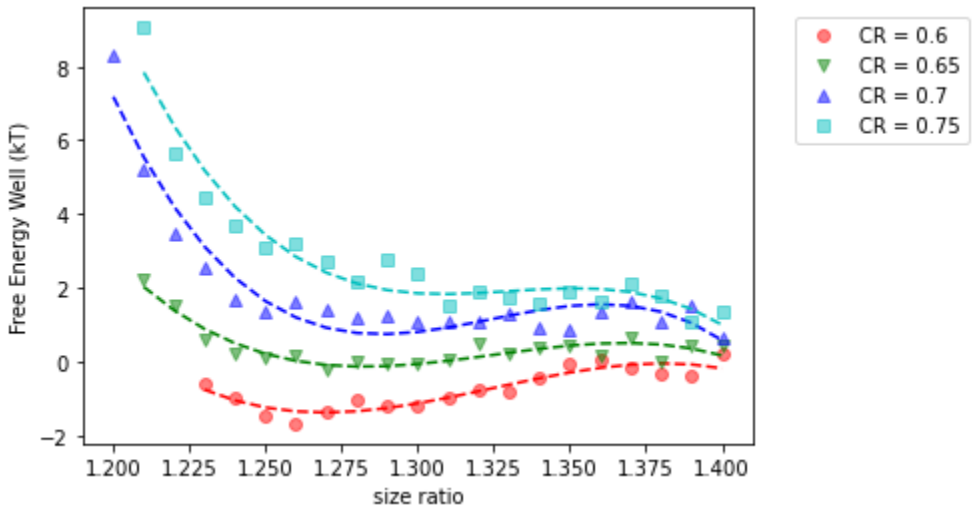

Figure 7: Local free energy well of binding for various compression ratios (CRs). The free energy

8 Bond Angle Distribution

The width of the WF potential is 20nm. However, the width of the free energy minima becomes wider as the size ratio of the cluster increases. The widening is due to the bond angle of the tetrahedra. For example, when the patch is too protruded beyond the lobe-lobe interlock distance, the bond can bend until it touches the lobes of another cluster. The bonding angle depends on the torsion angle of the tetrahedra. When the bonding orientation is staggered, the bond can bend more, widening the free energy well. When the bonding orientation is eclipsed, the bond cannot bend as much because of the lobes.

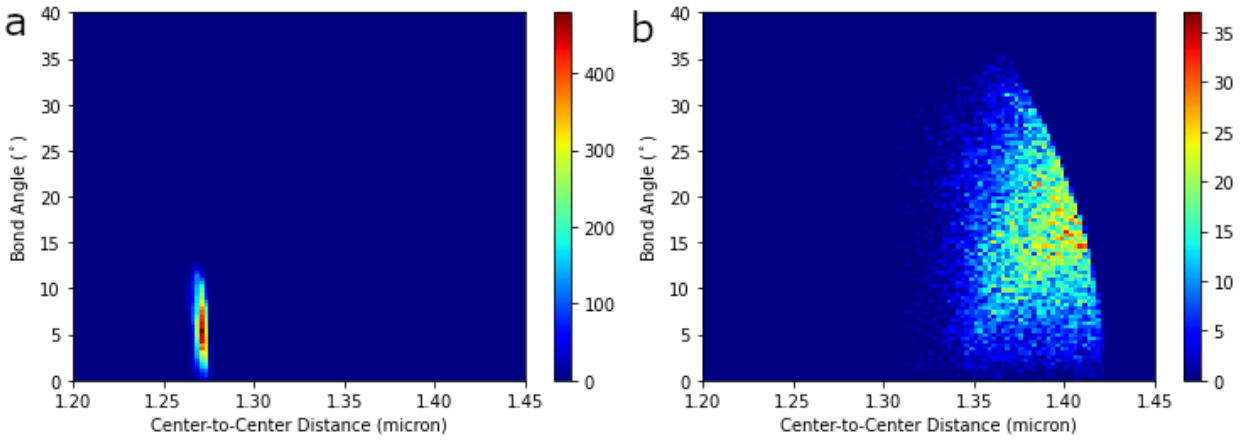

Figure 8: Bond angles and center-to-center distances capable of being explored by two bound tetrahedra with compression ratio 0.75 and size ratios 1.25 (a) and 1.40 (b). At larger size ratios, two bound particles are not as tightly interlocked and can explore a wider range of bond angles and center-to-center distances.

9 Gravity Induced Concentration Gradient

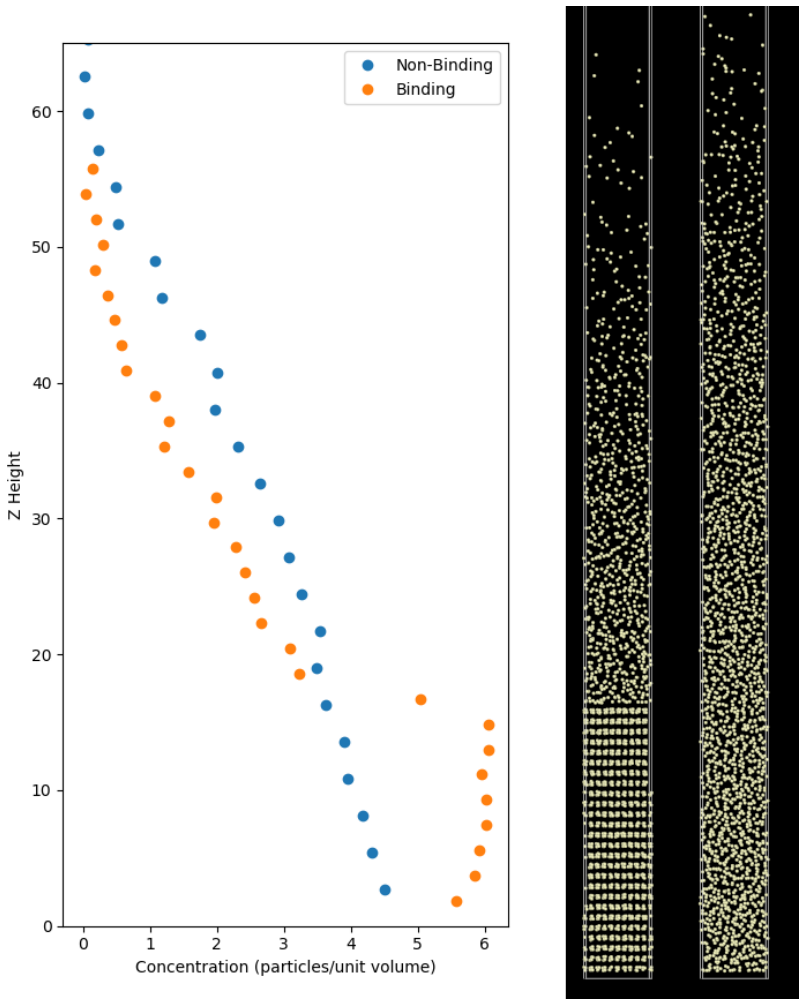

Figure 9: Concentration of TLPPs as a function of height in z for two different simulations of the same geometry (Compression 0.70 and size ratio 1.32): one where the particles are capable of binding and crystallizing, and one where the interactions are too weak for the particles to bind. Since the geometries are the same, any difference between the concentrations of the two systems is due to the crystallization. The terminal concentration that the crystal grows to can also be seen at the concentration where the curves cross, which is determined by the chemical potential.

10 Polydisperisty of TLPP Size

To grasp the robustness of the crystallization of TLPPs, molecular dynamic simulations were run with two types of particles: (1) particles of the standard size of 1-micron lobe (red) and (2) particles whose size is enlarged by a factor of 1.16 or 1.2 (blue) from type 1 particles. The simulations were run with 1:1 ratio of type 1 and type 2 particles. In all of the simulations, the compression ratio was 0.7, and the size ratios were 1.25, 1.30, 1.35, or 1.40. One of the final simulation snapshot is shown in Figure 10.

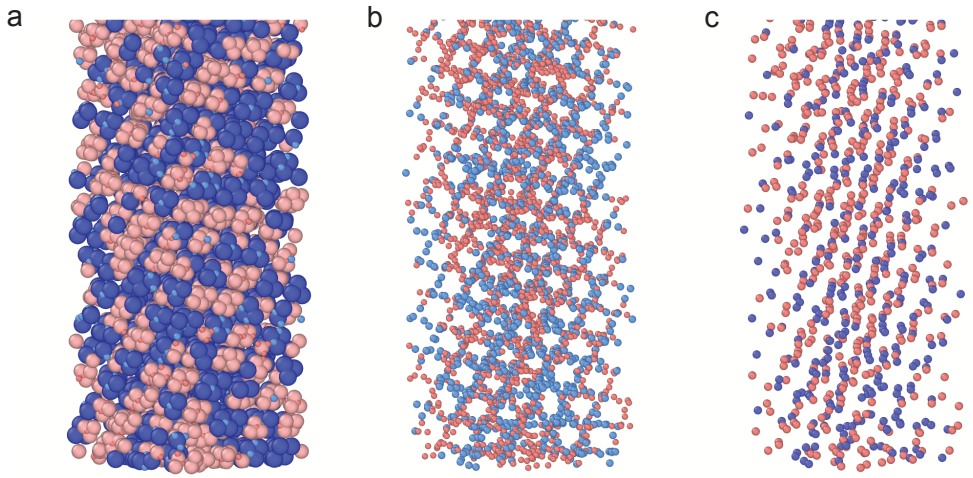

Figure 10: Final snapshot of MD simulation for a polydiserpse system. The TLPPs have a compression ratio of 0.7 and a size ratio of 1.30. The blue particles are bigger than the red particles by a factor of 1.2. (a) The final snapshot of the entire TLPPs. (b) The final snapshot of the patches of the TLPPs. (c) The final snapshot of the center of mass positions of the TLPPs.

In the monodisperse simulations, the TLPPs with a compression ratio of 0.7 crystallized with size ratios ranging from 1.26 to 1.38. In the polydisperse simulations, the TLPPs with a compression ratio of 0.7 and size ratio of 1.40 remained amorphous. Surprisingly, the TLPPs with a compression ratio of 0.7 and a size ratio of 1.25 crystallized, which did not crystallize in the monodisperse simulations. This indicates that the crystallization of TLPPs into the cubic diamond structure is robust against polydispersity and, in the case of the lower size ratio, can enhance the crystallization.

11 Patch Size

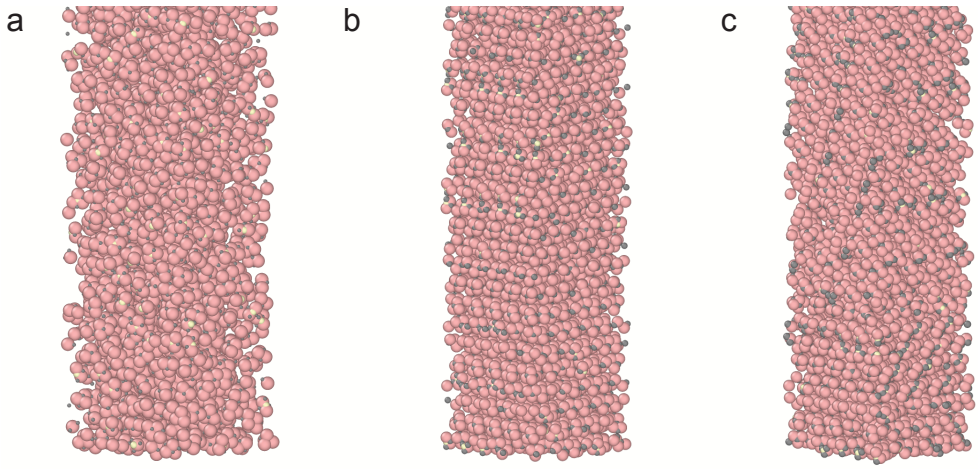

Figure 11: Final snapshot of MD simulation with varying patch size for TLPPs with compression ratio of 0.7 and size ratio of 1.30. (a) Patch size reduced by a factor of 0.7. (b) Patch size enlarged by a factor of 1.3. (c) Patch size enlarged by a factor of 1.5

References

(1) Glaser, J.; Nguyen, T. D.; Anderson, J. A.; Lui, P.; Spiga, F.; Millan, J. A.; Morse, D. C.; Glotzer, S. C. Strong scaling of general-purpose molecular dynamics simulations on GPUs. *Comput. Phys. Commun.* **2015**, *192*, 97–107.

(2) Hueckel, T.; Hocky, G. M.; Palacci, J.; Sacanna, S. Ionic solids from common colloids. *Nature* **2020**, *580*, 487–490.